Détection de rayonnement à très basses Température

4ème Ecole d'Automne D'Aussois : Balaruc les Bains 14- 20 Novembre 1999

Transitions edge sensors

Martin Loidl

DRTBT 1999 - 12

Transition edge sensors

Superconducting phase transition thermometers

Martin Loidl - CEA Saclay

I. The SPT
   1. The principle
   2. The fabrication
   3. Materials
II. Detectors with SPT sensors
III. Detector readout with SQUIDs
   1. The SQUID
   2. Readout schemes
   3. Noise
IV. Applications & performance
   1. X-ray detection - materials analysis
   2. X-ray astronomy
   3. UV / optical / IR astronomy
   4. Miscellaneous
   5. Dark matter search

I . SPT - the principle

Superconducting thin film, **weakly thermally coupled** to a **heat sink;** stabilized in the phase transition between normal conducting and superconducting state.

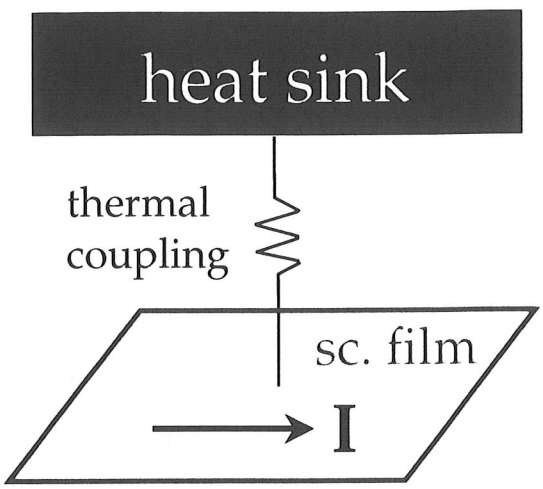

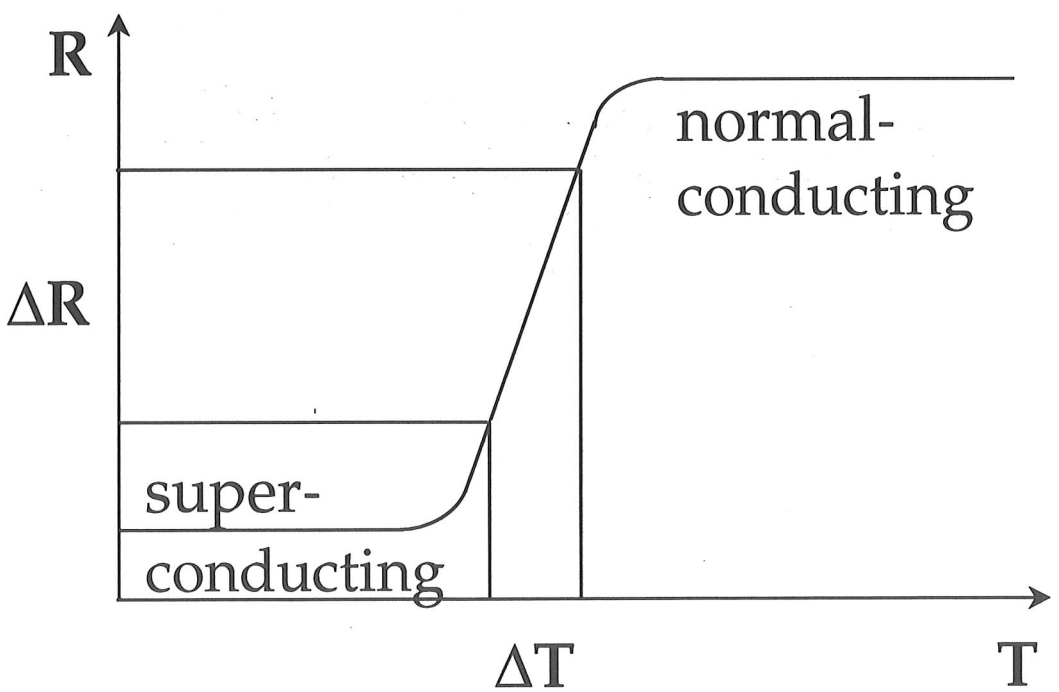

$T_C \lesssim 100$ mK

$\Delta T_C \sim 0.1 \ldots 10$ mK

$R_{nc} \sim 10 \ldots 100$ mΩ

$I \sim 1 \ldots 100$ μA

Weak thermal coupling

- provides cooling, but
- allows temperature excursions;
- defines time constant

$$\tau = C/G$$

C: heat capacity
G: thermal coupling

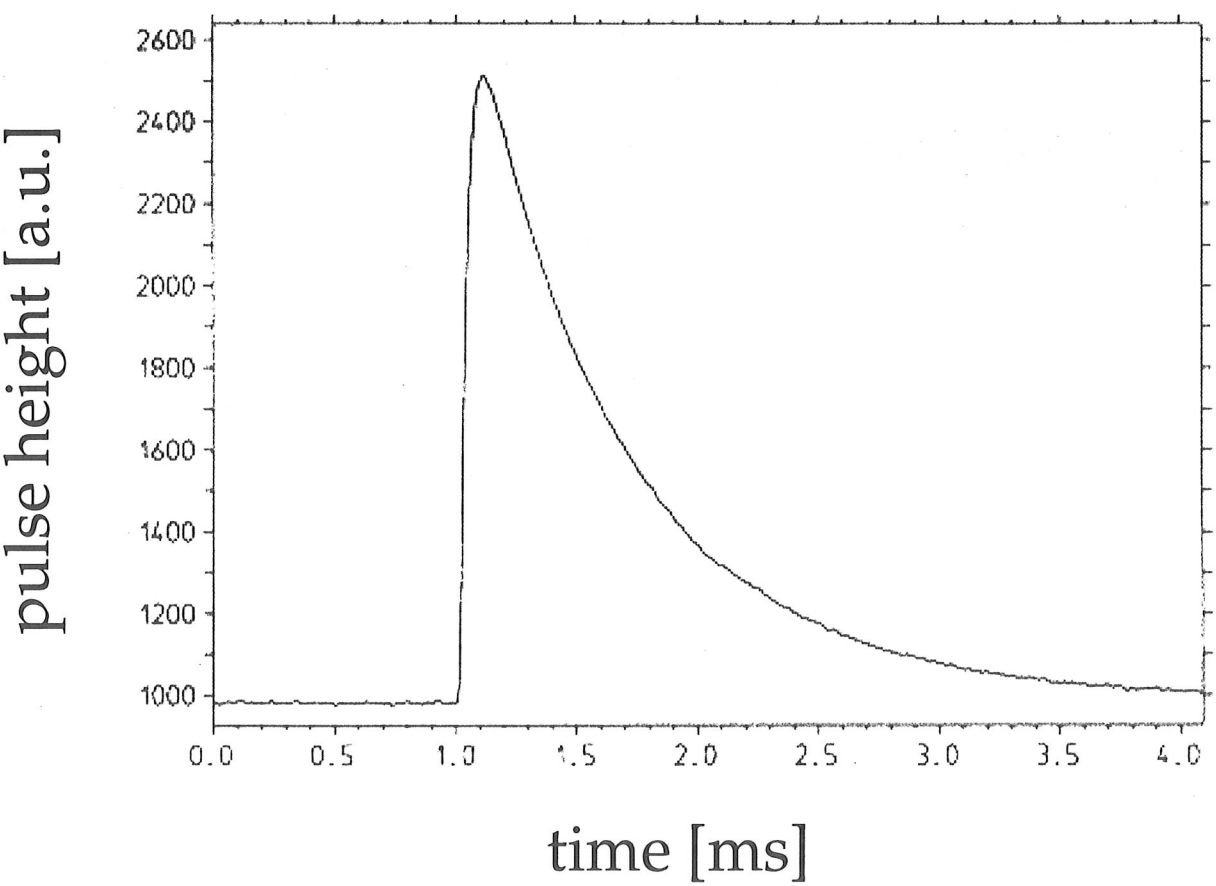

1 keV ⟶ ~ 10 ... 100 µK

sharp transition $\Rightarrow$ high sensitivity
linear transition $\Rightarrow$ linear response

Limitation of steepness and linearity by

Dependence of T_C on impurities; inhomogeneities of impurities $\Rightarrow$ areas of different T_C . Some materials: different crystalline phases favoured by impurities.

Dependence of T_C on film thickness.

Dependence of T_C on film stress.

Critical current density at film edges.

Bad edge structure.

Current density profile calculated for a 1 mm wide x 400 nm thick film:

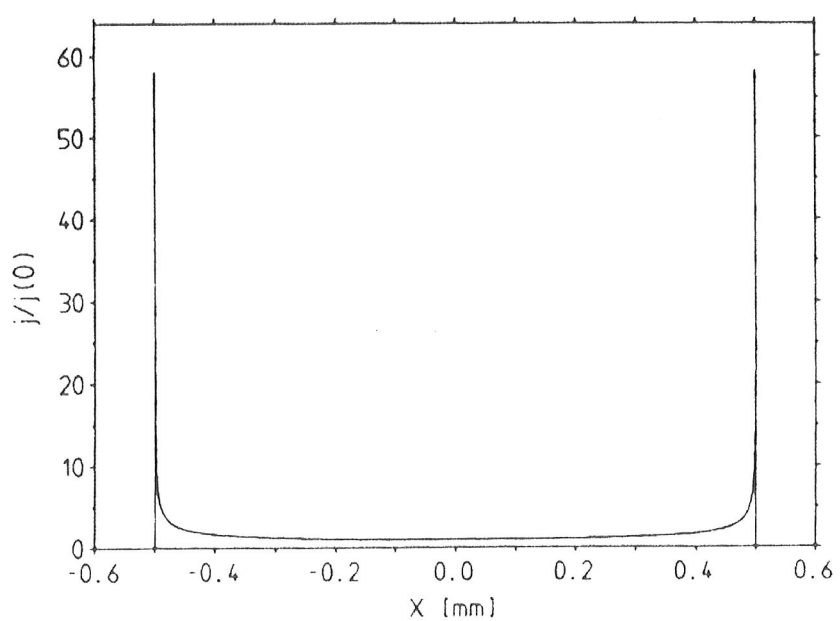

Film purity and morphology very important for the quality of the phase transition.

Possible ways to overcome the critical current limitation:

- Circular shape:

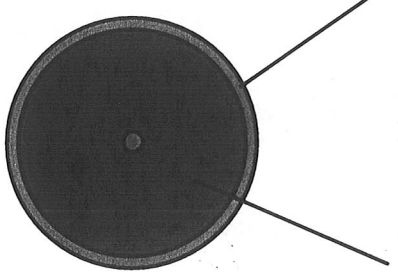

superconducting ring contact with higher T_C than thermometer; current flows from center to circumference

circular thermometer

No edges ⟹ homogeneous current density, but low normalconducting resistance.

- Increase the number of edges:

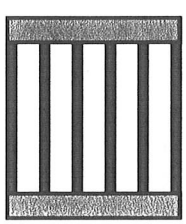

n strips:
current density per edge is reduced by a factor **n**

I .2 SPTs - the fabrication

- Cleaning!

- Deposition
  Rf- or dc-sputtering (cheaper, simpler) or electron-beam evaporation in UHV (cleaner).
  The lower T_C, the more sensitive to impurities
  $\Rightarrow$ low-T_C films mostly evaporated.

- Structuring

deposition through a
<u>shadow mask</u>
- simple
- low precision
- no fine structures
- not very clean

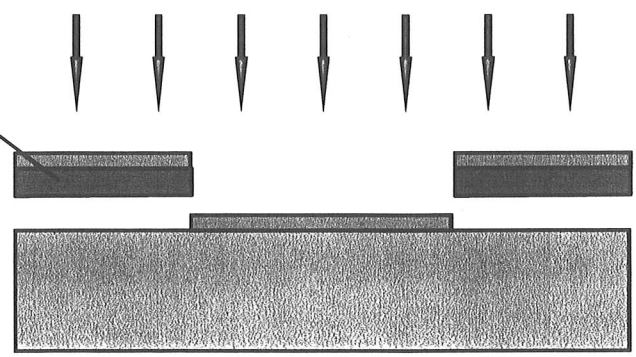

Photolithography

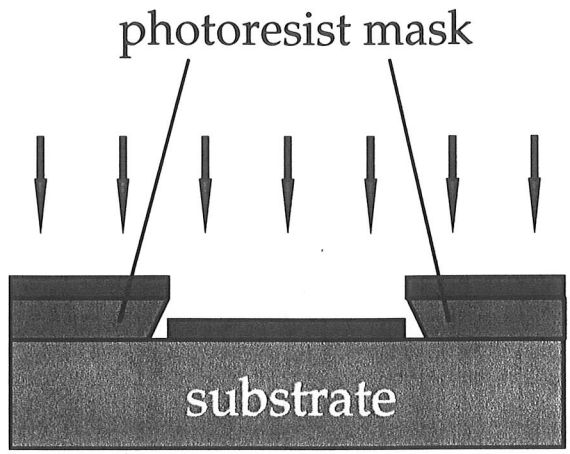

- liftoff mask
  - good edge definition
  - moderate cleanliness
  - no very high substrate temperatures

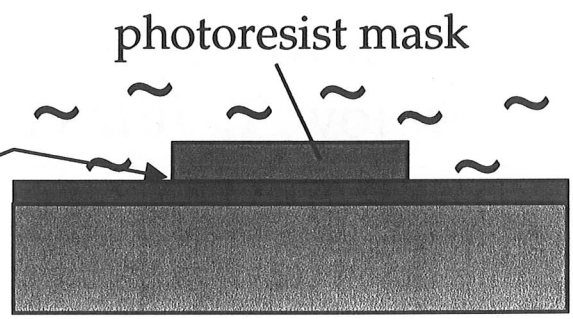

- wet chemical etching
  - often good results
  - clean process
  - underetching possible
  - not applicable to some noble metals

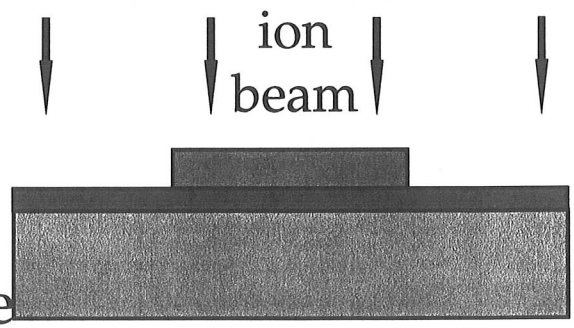

- sputter etching
  - good edge definition
  - applicable to all metals
  - substrate surface damage

Contacts

- thin film leads: Al, Nb
- bonding wires: Al, Au

I .3 SPTs - materials

- Superconducting elements with low T_C

Cd	517 mK	used for first SPT
Hf	128 mK	rare earth (purity?), but considered for STJs
Ir	112 mK	used by several groups
Be	26 mK	in thin films $T_C > 5K$
W	15 mK	MPI Munich
	> 70 mK	Stanford / Berkeley; T_c can reproducibly be lowered by Fe implantation down to ~ 50 mK.

- Alloys / intermetallic compounds

with T_C ~ 100 mK exist (Ag_4Sn, Al_2Au, Sn_xTe_{1-x}). Difficult to produce homogeneous films, at present not used for SPTs.

- Proximity bilayers

Bilayers of a superconducting and a normal metal; T_C (bilayer) < T_C (superconductor).

Proximity effect:

Finite coherence length of Cooper-pairs
⇒ Cooper-pairs can enter normal conductor
⇒ Superconductor: Cooper-pair density drops, electron-electron interaction effectively weakened ⇒ T_C drops.
⇒ Normal conductor: presence of Cooper-pairs ⇒ superconducting.
If film thickness < coherence length ξ:
T_C ~ constant throughout the whole bilayer, can be adjusted by the ratio of film thicknesses.

Theories need (at least) one free parameter.
Two models (Werthamer: semiempiric, Usadel: microscopic theory) predict T_C and I_C quite well.
⇒ After detemining free parameter films with a desired T_C (± few mK) can be made.

Proximity bilayers: fabrication

Important to avoid interdiffusion or formation of compounds at the interface

⟹ not all metal combinations possible,

⟹ substrate temperature for 2nd deposition restricted.

Good metallic contact at interface essential

⟹ remove possible oxide layer before 2nd deposition.

Metal combinations:

Al/Ag

T_C (Al) = 1.175 K
T_C (Al/Ag) ~ 50mK - 1 K,
reproducible within 2 mK
ΔT_C ~ 0.1 mK
Stable, if structured by shadow mask; but unstable, if structured by photo-lithography (shift in T_C, increasing R_{nc}).

β-Ta/Ag

T_C (β-Ta) ~ 600 mK
no lowering of T_C observed

Ti/Au

T_C (Ti) ~ 390 mK
two groups: T_C (Ti/Au) > T_C (Ti) !
SRON: T_C (Ti/Au) ~ 150 mK in use.

Mo/Au

T_C (Mo) = 915 mK
T_C (Mo/Au) ≥ 100 mK
$\Delta T_C \leq 1$ mK

Mo/Cu

LLNL: multilayers,
few nm each layer $\ll \xi$
$\Longrightarrow$ no limit of total thickness,
sharp transition, $T_C > 40$ mK
NIST: bilayers, $T_C \sim 100$ mK,
normal conducting Cu side banks
for defined edge conditions, but
additional heat capacity ($d \gg \xi$).

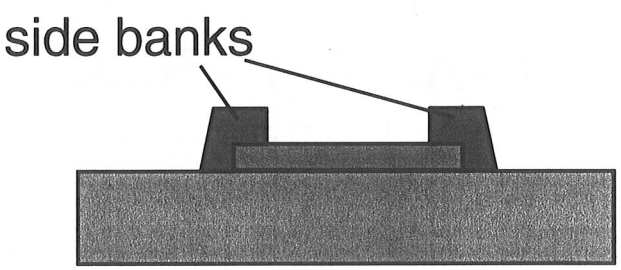

Ir/Au

T_C (Ir) = 112 mK
T_C (Ir/Au) = (17) ... 25 - 100 mK
predictable within few mK
$\Delta T_C < 1$ mK
perfectly stable
only ion beam structuring

II. Detectors with SPT sensors

The basic concepts

Calorimeter: measures energy deposit of individual photons or particles

Bolometer: measures an energy flux

- Monolithic calorimeters/bolometers
  - absorber = thermometer
  - for low energies < 1 keV
  - thermal coupling: thin Si_3N_4 membrane

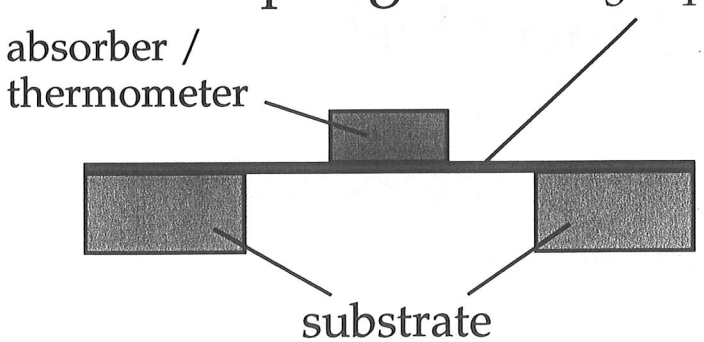

  - energy transfer directly to the free electrons

$$\Delta T = \Delta E / C_{th}$$

- Composite detectors: microcalorimeters

- SPT sensor + normal- or semimetal absorber

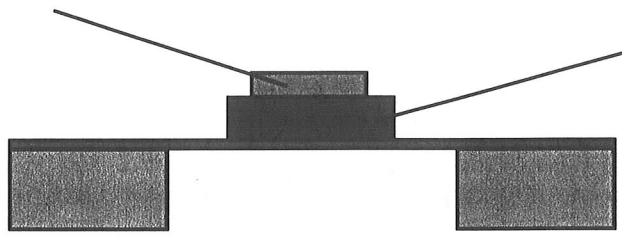

- free choice of absorber and thermometer materials
- thermal coupling mostly Si_3N_4 membrane
- energy transfer to free electrons of absorber, good thermal contact with thermometer electrons

$$\Delta T = \Delta E / (C_{abs} + C_{th})$$

- Composite calorimeters with dielectric absorbers

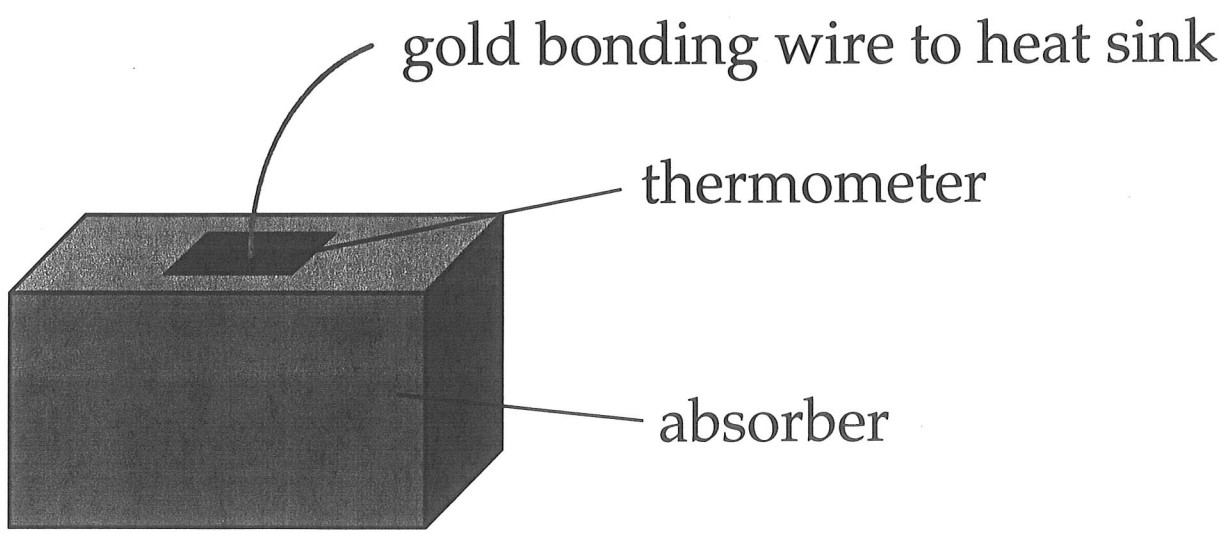

Particle interaction creates nonthermal phonons in the absorber which are collected by the SPT.

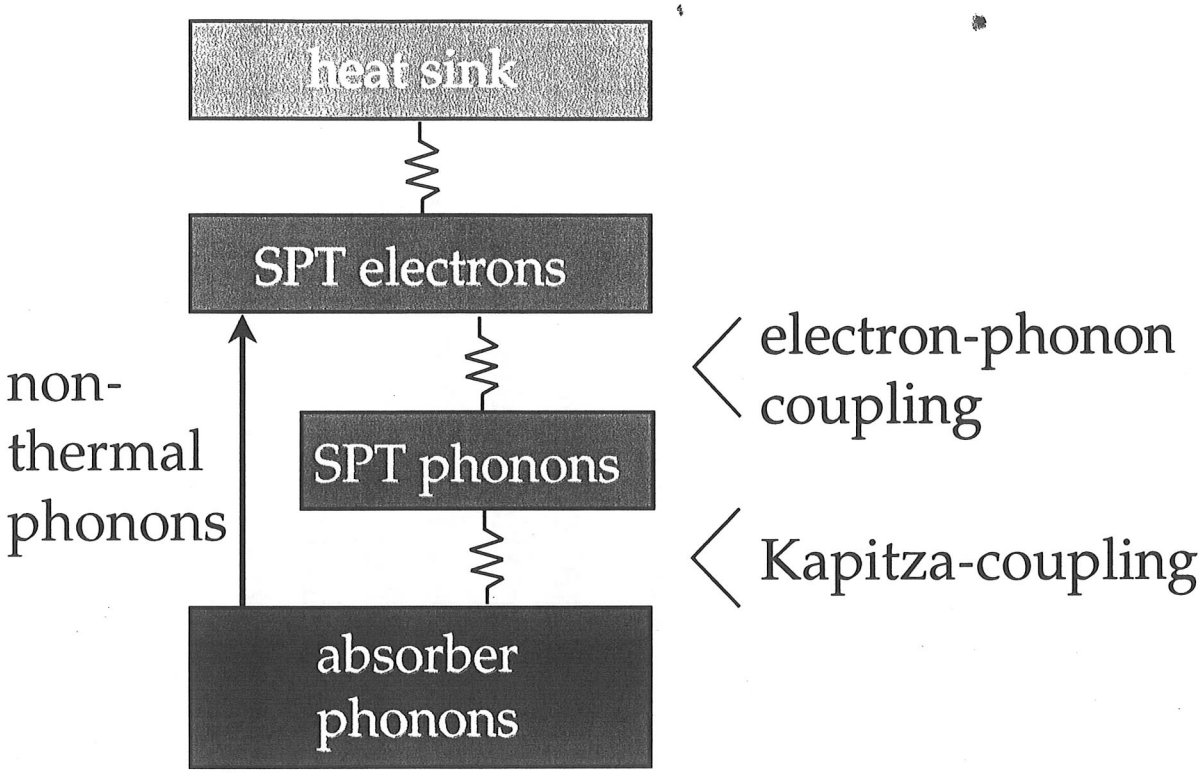

Electron-phonon coupling ~ T^5 ... T^4,
very weak well below 100 mK

⟹ SPT thermally decoupled from absorber.

⟹ Nonthermal phonons heat directly the SPT but not the absorber.

$$\Delta T = \Delta E / C_{th}$$

⟹ use of large mass absorber without loosing much in sensitivity.

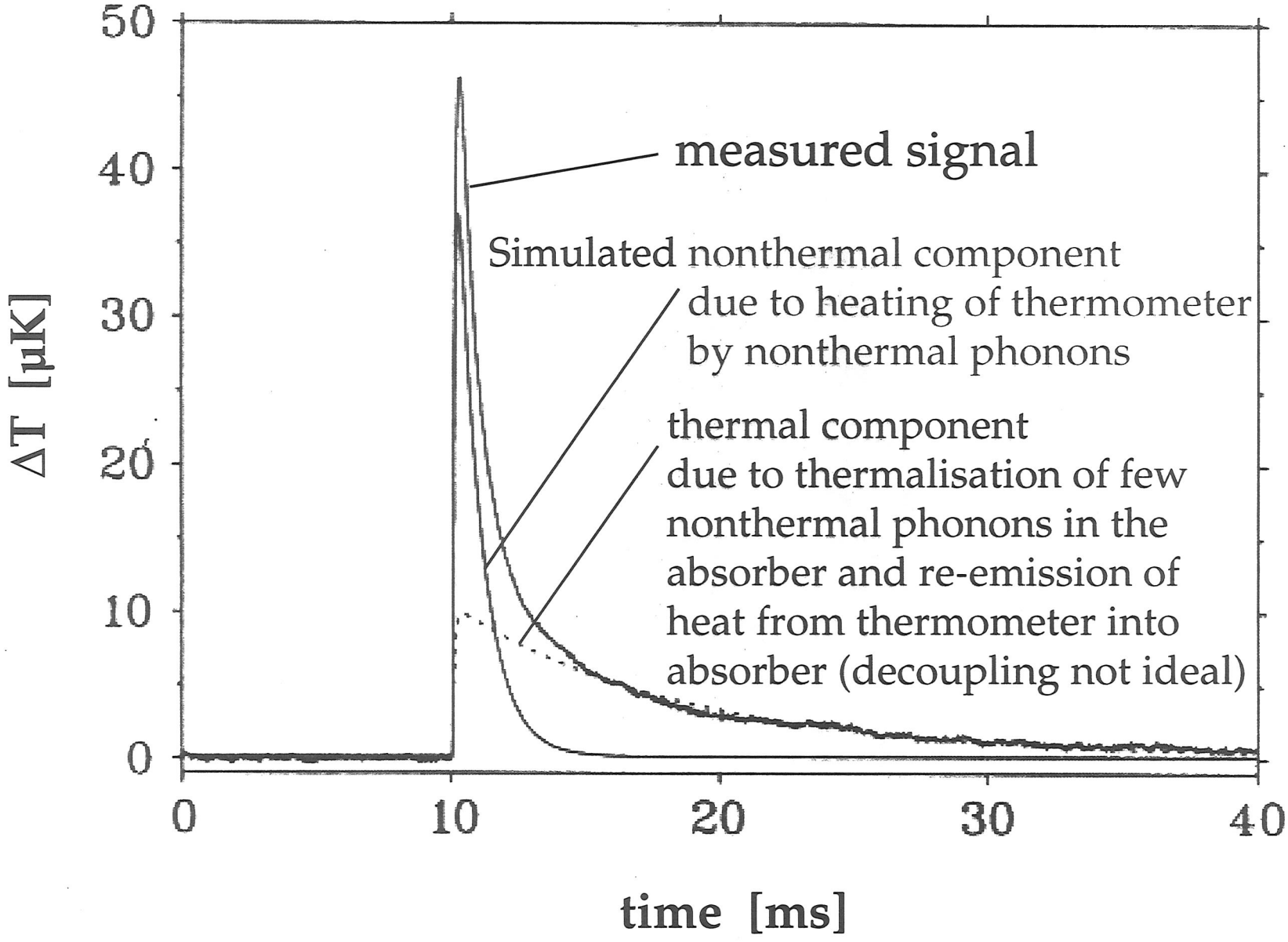
50
40
30
20
10
0
ΔT [μK]
0
10
20
30
40
time [ms]
measured signal
Simulated nonthermal component
due to heating of thermometer
by nonthermal phonons
thermal component
due to thermalisation of few
nonthermal phonons in the
absorber and re-emission of
heat from thermometer into
absorber (decoupling not ideal)

Phonon collectors

To avoid thermalisation of nonthermal phonons in the absorber: fast collection.

Fast collection requires large collecting area:

$$\tau_{coll} \propto V_{abs} / A$$

Small heat capacity $\Longrightarrow$ small thermometer

Solution:

Small SPT + superconducting phonon collector film with T_C (coll.) $\gg$ T_C (SPT).

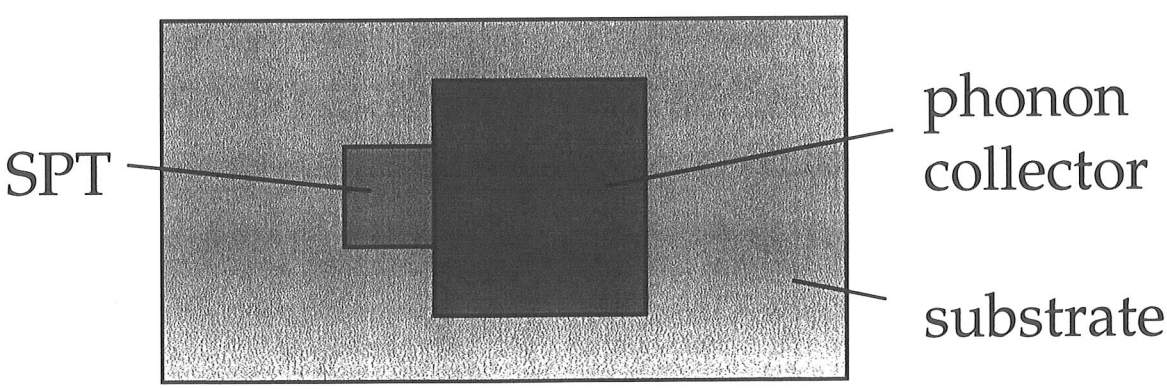

Nonthermal phonons break up Cooper-pairs into quasiparticles (QP).
QP diffuse through collector and are trapped in the SPT.
Energy release to SPT electrons $\Longrightarrow$ heating.

III. Detector readout with SQUIDs

III.1 The SQUID - Superconducting Quantum Interference Device

- Amplifier for low impedant signal sources
- Primarily extremely sensitive magnetometer
- Current coupled to the SQUID by a coil which converts the current into a magnetic field.

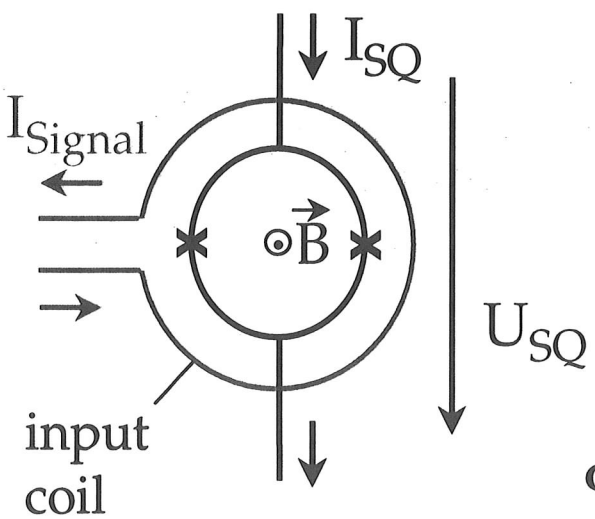

superconducting ring with two Josephson junctions; phase correlation between 2 halves $\Rightarrow$

$$U_{SQ} \propto sin\,(2\pi\Phi/\Phi_0)$$

Φ: flux through SQUID loop

$\Phi_0 = h/(2e) = 2.07 \times 10^{-15}\ Tm^2$

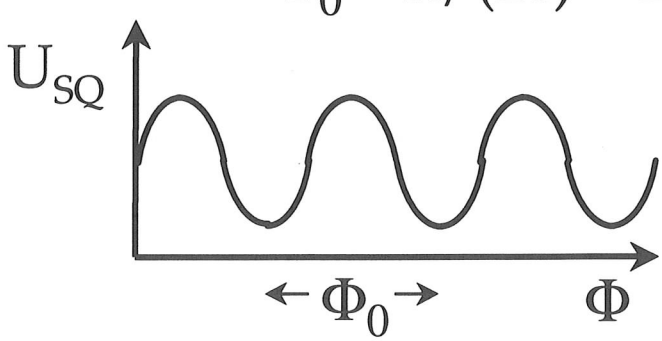

No absolute measurement !

Amplitude of U_{SQ} typically ~ 30 µV,

maximal slope ~ 100 µV/Φ_0,

sensitivity ~ 150 nA ... 15 µA /Φ_0.

To linearise U_{SQ} /I and to increase the measurable range: magnetic feedback maintains flux through the SQUID constant.

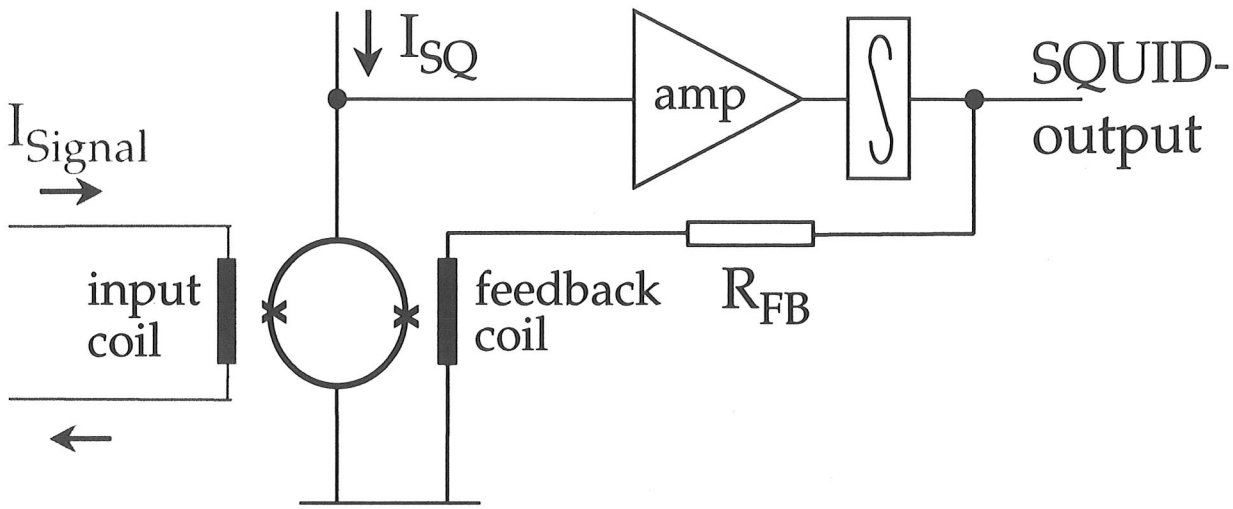

Mostly operated in modulation/demodulation mode, modulation frequency limits bandwidth: commercial systems ~ 30 kHz - 2 MHz.

«Slew rate»: maximal rate of signal variation dI/dt, limited by SQUID electronics. ~ 10^4 - 10^6 Φ_0 /s. If exceeded: «flux loss», i.e. loss of information about signal amplitude.

SQUID arrays: ~ 100 - 200 SQUIDs in series
⇒ output voltage ~ 10 mV.

2-stage SQUID arrays: output of a single SQUID is read out by a SQUID array.

III.2 Readout Schemes

Basic readout circuit:

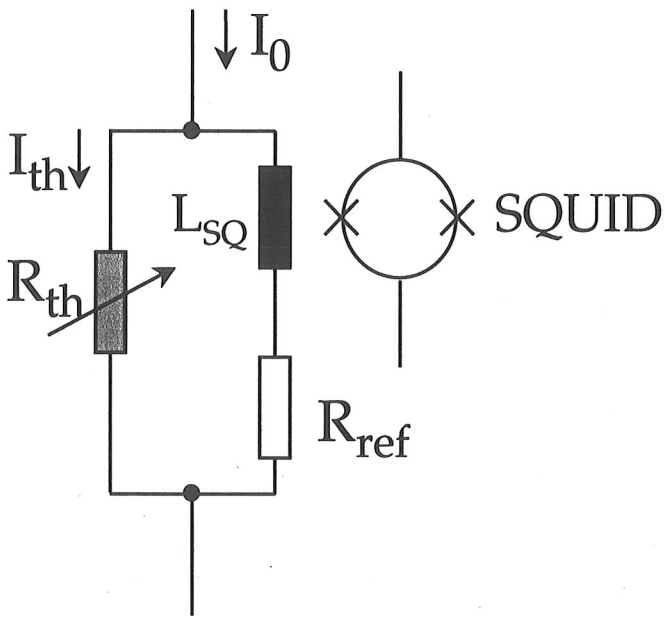

Low resistances
$\Longrightarrow$ superconducting wiring.

Also SQUID input coil usually superconducting.

SQUID measures branching ratio of current I_0.

Highest signal amplitude: $R_{ref} = R_{th}$.

But power dissipation of measuring current $I_{th}^2 R_{th}$ together with weak thermal coupling

$\Longrightarrow$ self heating $T_{th} > T_{bath}$

Current bias $\Longrightarrow$ positive feedback
$\Longrightarrow$ thermal fluctuations are enhanced, at high I_{th} unstable operation.

Electrothermal feedback (ETF)

$R_{ref} \ll R_{th}$:

voltage bias $\Longrightarrow$ power dissipation V^2 / R_{th}

$\Longrightarrow$ negative «electrothermal feedback»

- temperature excursion reduced
- thermal fluctuations & current noise damped
- faster relaxation:

$$\tau = \tau_0 / (1 + \alpha/n)$$

$\alpha = d\,log\,R / d\,log\,T$ «logarithmic sensitivity» of SPT

$n = d\,log\,P / d\,log\,T$ $(P = V^2 / R_{th})$

- shorter pulses, higher count rate
- almost constant operating point

$\Longrightarrow$ better linearity, wider dynamic range

Feedback effect depends on R_{th} / R_{ref}, G, and V (i.e. measuring current).
What is measured in the ETF regime is the reduction of the measuring current.

Active thermal feedback (ATF)

Additional heater on the SPT, feedback circuit controls heating power such that T_{th} = const.
$\Longrightarrow$ power input from event is removed by reducing the heating power.

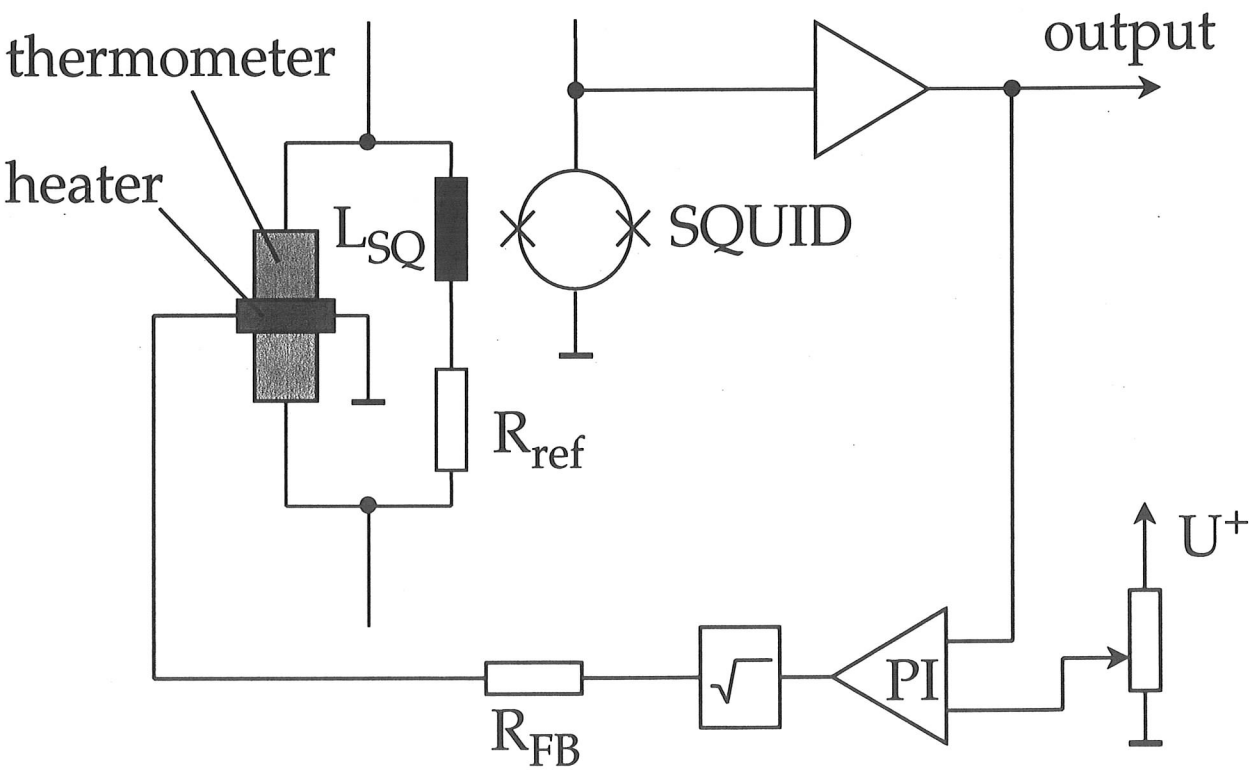

Heater:
- gold bonding wire (thermal coupling)
- gold thin film in thermal contact with SPT

What is measured in the ATF regime is the reduction of the heating power.

Active thermal feedback: advantages

- potentially stronger than ETF
- better temperature stabilisation
  $\Longrightarrow$ all advantages of ETF can be improved
- no limitation of heating power by critical current through thermometer
- heating current and measuring current independent $\Longrightarrow$ additional degree of freedom in operation
- SQUID included in feedback loop
  $\Longrightarrow$ additionally to thermal fluctuations and current noise also SQUID noise is reduced (may be dominant at very low T).

Similar concept with a normal metal absorber used as heater proposed by a Japanese group, no results yet.

III.3 Noise

- **Thermodynamic noise**

  Temperature fluctuations by statistical energy exchange with the heat bath through G.

$$NEP = \sqrt{4\, k_B\, T_C^2\, G}$$

- **Johnson noise**

  Random scattering of electrons in R_{th}, R_{ref}.

$$NEP = \sqrt{4\, k_B\, (T_C\, R_{th} + T_{ref}\, R_{ref})}\ /|S|$$

$$S = \Delta V_{th}/P$$

- **SQUID noise**

  Strongly dependent on design of SQUID («flux noise») and its insert («SQUID probe») in the cryostat. Can dominate the total noise at very low T.

  Typically 1 - 30 $pA/\sqrt{Hz}$

- **1/f - noise**

  Caused by
  - grain boundaries
  - edge effects
  - contact resistances

  Careful sample preparation $\Longrightarrow$ negligible.

- **Bolometers**

$$S/N = P_{signal}/NEP$$

$$NEP_{tot} = \sqrt{(NEP_{therm})^2 + (NEP_{John})^2 + (NEP_{SQ})^2}$$

$$\sim 10^{-15} - 10^{-18}\ W/\sqrt{Hz}$$

- **Calorimeters (with ETF)**

$$\Delta E_{FWHM} = \sqrt{k_B T_C^2 C \sqrt{8n}/\alpha}$$

$$\sim 100 - 0.1\ eV$$

Less than sum of contributions without ETF («thermodynamic limit»), but excludes SQUID noise.

Theoretically no dependence on energy.
In practice ΔE_{FWHM} increases with E due to energy loss, excitation of metastable states ...

Additional resolution degrading effects

- Unstable operating point due to pile-up or thermal fluctuations of heat bath in conjunction with
  - nonlinearities in phase transition
  - $C_{th} = C(T)$ in the transition
  - $G = G(T)$

  ⟹ avoid too high count rates,

  ⟹ temperature stabilisation 1 - 0.01 μK of cryostat, better of detector holder.

- Microphonics

  ⟹ as for all LTDs: vibration damping, fix all wires ...

- Electromagnetic pickup

  ⟹ best: Faraday cage, filtering of all electric leads in/out, and magnetic shielding (cryoperm).

IV. Applications & performance

IV.1 X-ray detection - materials analysis

E ~ 100 eV ... 10 keV

Conventional detection:

- Energy dispersive semiconductor detectors at LN_2 - temperature (77K):
  ionisation; charge separation by electric field,

  $\Delta E \sim 130$ eV, count rate ~ 3000 s^{-1}
  ~ 175 eV, ~ 30000 s^{-1}

- Wavelength dispersive spectrometers:
  Bragg-reflection on diffraction crystals,

  $\Delta E \sim 2$ - 20 eV, count rate ~ 50000 s^{-1}

  but only one wavelength at a time
  $\Rightarrow$ time consuming scan over whole energy range

LTDs: high energy resolution + count rate

SPT-microcalorimeter designs

1. Normal metal absorber, small overlap with a small SPT

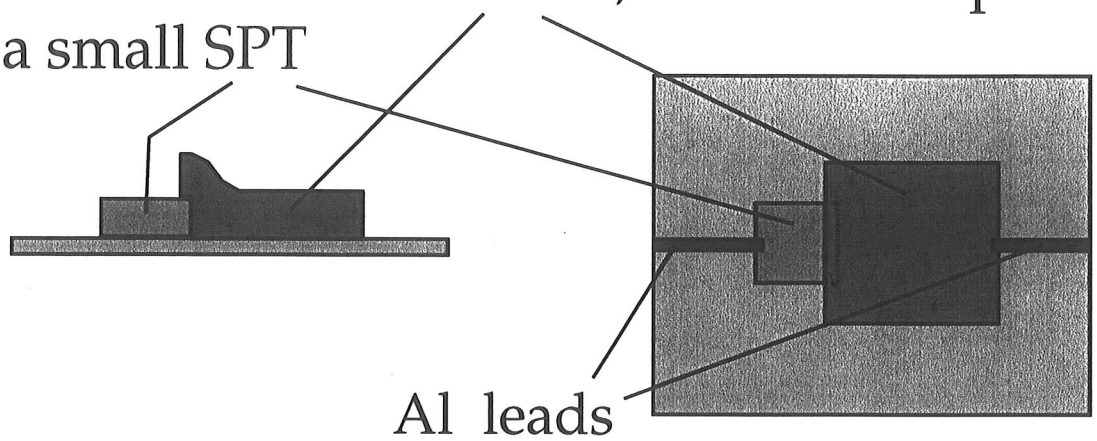

2. Absorber on backside of Si_3N_4 membrane
   thermal coupling absorber - SPT by phonons
   $\Longrightarrow$ only efficient for $T \gtrsim 100$ mK !

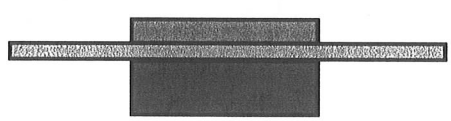

3. Small normal metal absorber on top of SPT
   $\Longrightarrow$ small part of SPT normal conducting.
   Unproblematic, current carried by edges,
   but small acceptance area.

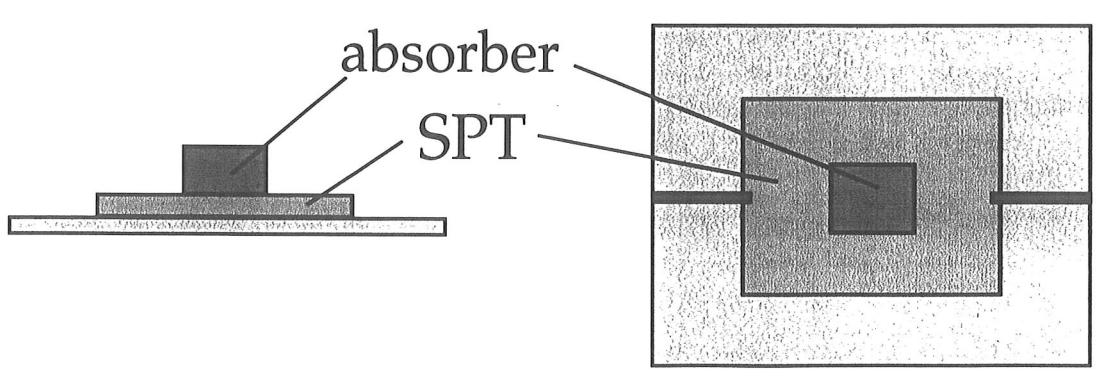

4. Absorber of aqual area as SPT on top of SPT: possible, if absorber is poor electrical conductor or has semimetallic character, e.g. Bi.
Larger acceptance area than (3), fast response.

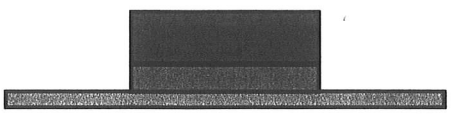

Small acceptance areas of microcalorimeters
⟹ use of polycapillary X-ray optics.

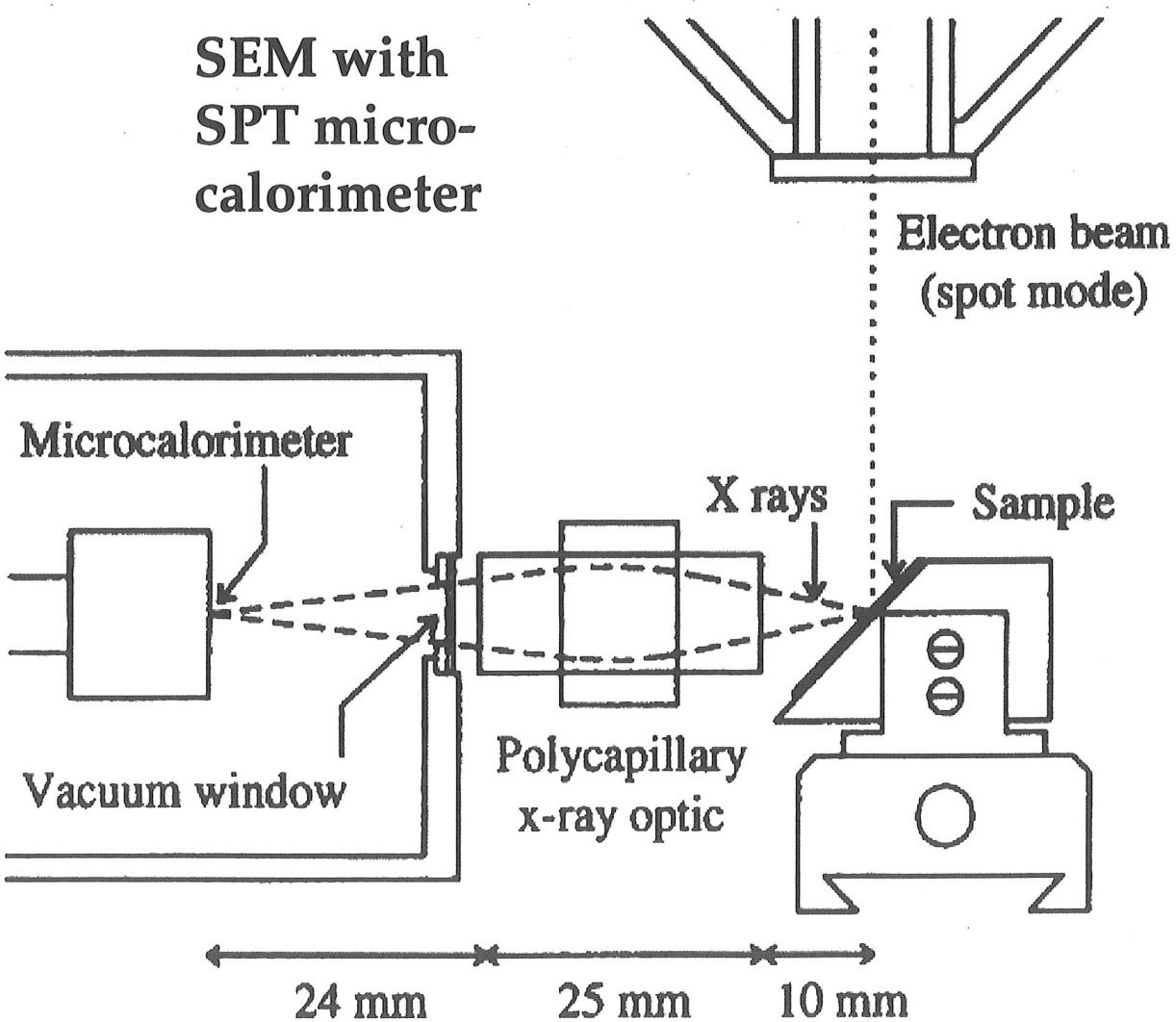

X-ray microcalorimeters - best resolutions

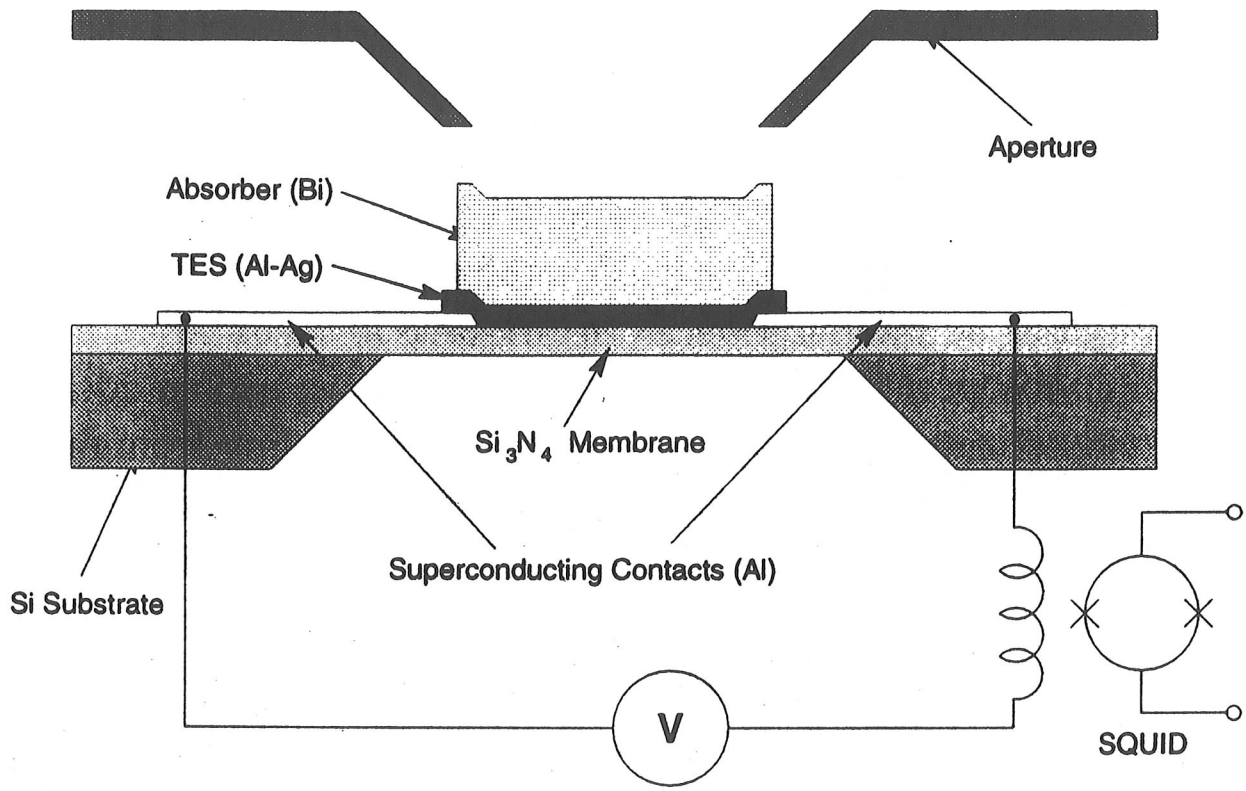

NIST, Boulder, Colorado

Al/Ag SPT, 400 x 400 μm² x 300 nm, T_C = 120 mK
Bi absorber, equal area x 2 μm
Quantum efficiency @ 6 keV > 75%

$$\Delta E_{FWHM} = 2.0 \text{ eV} \ @ \ 1.5 \text{ keV}$$

Theoretical: ΔE_{FWHM} ~ **0.5 eV** for ETF (α = 1000),
«thermodynamic limit» ~ **10 eV.**
Maximal count rate ~ **500 s^{-1}.**

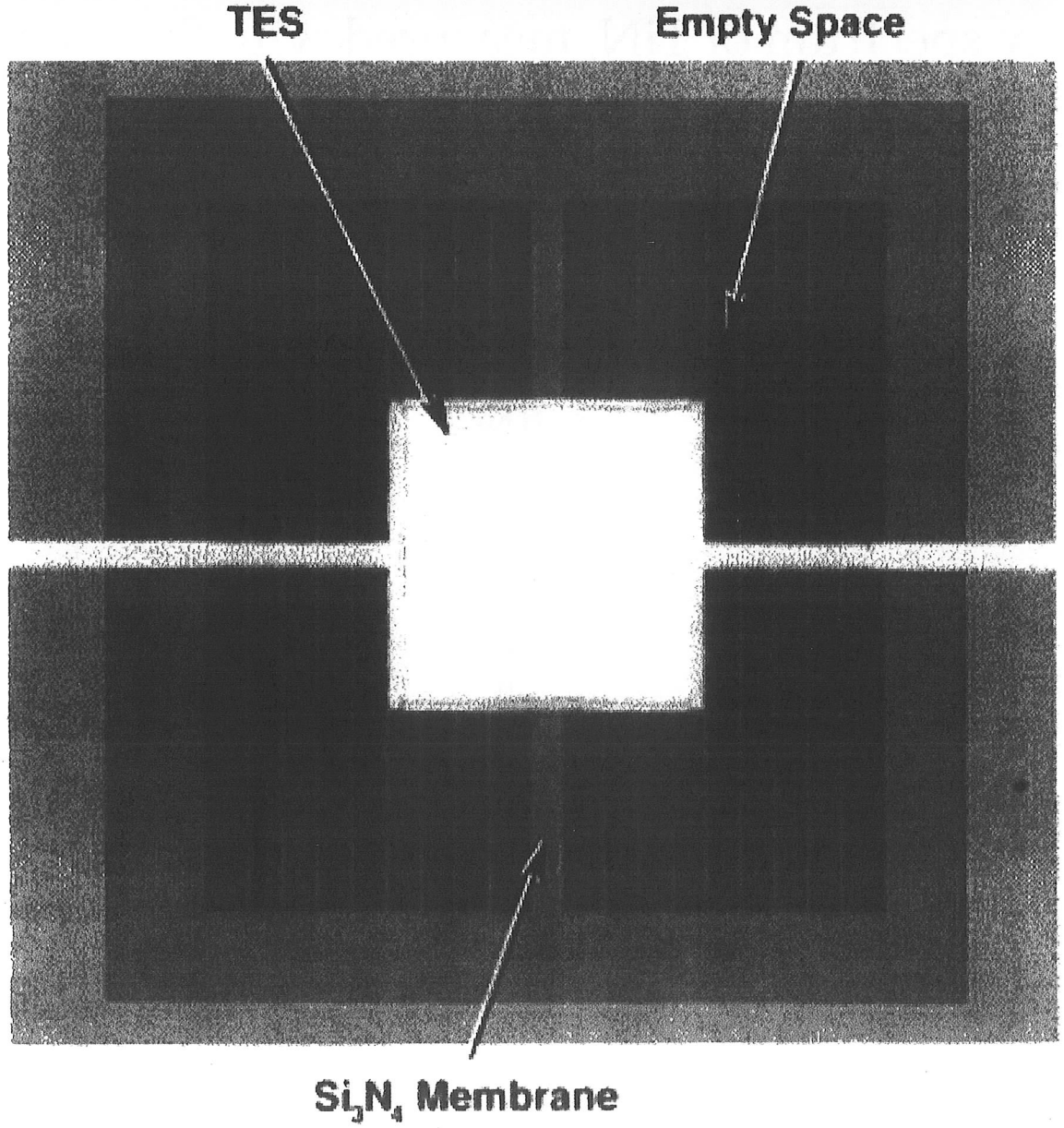

NIST, Boulder, Colorado

Mo/Cu SPT, 400 x 400 µm², 60 nm Mo + 200 nm Cu
no absorber ⟹ quantum efficiency low

$$\Delta E_{FWHM} = 4.5 \text{ eV} \quad @ \quad 5.9 \text{ keV}$$

Maximal count rate ~ 500 s^{-1}.

X-ray spectrum of TiN, measured with the micro-calorimeter with Al/Ag SPT and Bi absorber, in comparison with a conventional semiconductor detector measurement

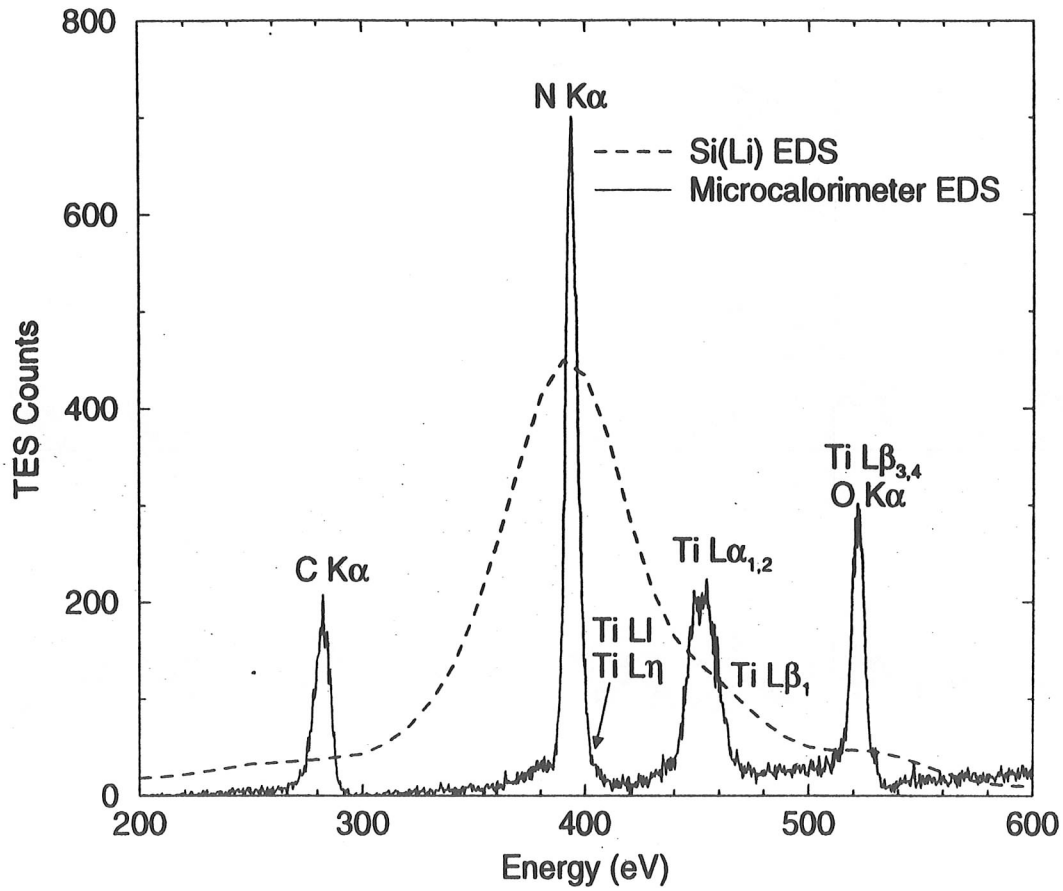

The Mn K_α–line, measured with the Mo/Cu SPT micro-calorimeter (without absorber), with a FWHM energy resolution of 4.5 eV.

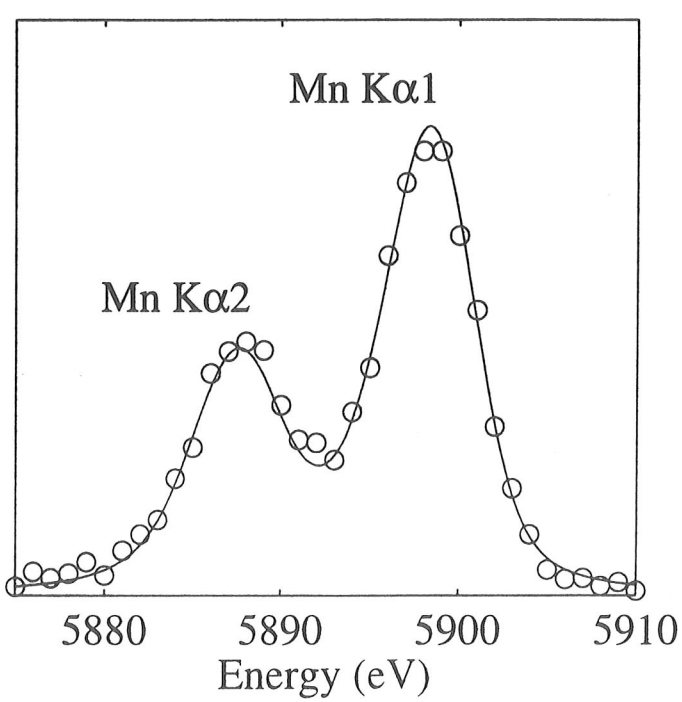

IV.2 X-ray astronomy

Requirements as for materials analysis, but additionally imaging capability needed
$\Longrightarrow$ multi-pixel arrays.

Conventional (Compton-) X-ray telescopes:

- low energy-, moderate spatial resolution,
- no energy-, higher spatial resolution.

Most advanced project using LTDs:

Several suborbital flights of a 36 pixel array of ion-implanted Si thermistors with HgTe absorbers, operated at 60 mK. (McCammon *et al.)*

ΔE = 10 - 14 eV @ 6 keV
8 - 11 eV @ 1 keV

First satellite mission in early 2000!

SPT-based LTDs

Several groups work on design and fabrication of SPT-arrays, but no results yet.

Alternative approach

Read out an extended absorber with 2 sensors at the ends $\Longrightarrow$ 1-dim. spatial resolution.

Superconducting absorber film

- X-rays create quasiparticles
- qp diffuse through the film and are detected in the sensors
- Pulse heights of correlated signals yield information about energy and position of absorbed X-ray photon.

STJ sensors

Good energy resolution ($\Delta E \sim 26$ eV),
but only for the center of the absorber.
Only small transport distances (few 100 µm).
Arrays of ~10 strips being prepared.
(Several groups)

W-SPT sensors, $T_C = 15$ mK

Poor energy resolution ($\Delta E \sim 150$ eV),
but ~ constant over whole length.
Transport distances up to 4 mm.
Slow quasiparticle diffusion.
(Large thermometers, massive substrate.)
(MPI Munich)

Dielectric absorber + W-SPT sensors

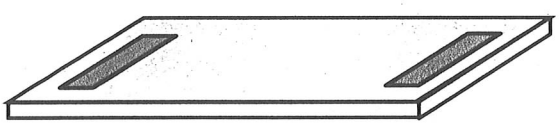

thin sapphire plate
2 W SPTs (15 mK)
up to 10 mm distance

- X-rays create nonthermal phonons.
- Diffusion of phonons by diffusive surface scattering.

$\Delta E = 216$ eV over 10 mm,
$\Delta E = 167$ eV within central 3 mm.

(Univ. of Oxford / MPI Munich)

IV.3 UV / optical / IR astronomy

E ~ 0.3 - 100 eV
no absorber needed

UV astronomy

- W SPTs, T_C = 75 mK
- 125 x 125 µm² x 35 nm
- quantum efficiency > 80% for 10 - 100 eV
- ΔE_{FWHM} = 3 - 8 eV

(Stanford University)

Near IR / optical astronomy

- W SPTs on Si or Ge substrates, T_C ~ 80 mK
- 20 x 20 µm² x 35 nm
- quantum efficiency 10% (IR) - 50% (optical)
- ΔE_{FWHM} = 0.15 eV @ 0.3 - 3 eV
- theoretically:
  ΔE = 0.037 eV (thermodyn.)
  0.088 eV (incl. energy loss to substrate)
- timing resolution ~ 100 ns
- count rate 30000 s^{-1}
- first real astronomical observation: Crab pulsar (using a single SPT)

- 6 x 6 pixel prototype array exists, but no measurement yet.
- Improvement of QE by «gold black» coating under investigation (few nm Au evaporated in a 1 mbar Ar atmosphere - heat capacity has to be checked):
  QE > 99% for 2 nm - 10 μm

(Stanford University)

Far IR / sub-mm astronomy

SPT acts as **bolometer**, i. e. measures a photon flux.
Potential of SPTs in a 32 x 32 pixel array is being evaluated in comparison with feed horn assisted NTD Ge thermistors and with ion-implanted Si thermistors.
(Queen Mary and Westfield College, GB)

IV.4 Applications - miscellaneous

Bio-molecule mass spectroscopy

Conventional:
Microchannel-plates, ionizing detectors.
Strongly decreasing efficiency for heavy, slowly moving molecules.

Time-of-flight mass spectrometers (TOF-MS) using SIN or SIS tunnel junctions in experimental phase since several years, yielding good results.

In next future, TOF-MS using SPTs will be developed for this application.
Potentially higher resolving power,
timing resolution ~ 100 ns expected.
(MPI Munich / Bruker Dresden)

Neutrino mass experiment

Measuring the tritium beta decay spectrum.
(Magnetic spectrometers used up to now:
unknown systematic errors.)
Tritium implanted in Au foil absorber,
thermally coupled to an Al/Ag SPT, $T_C = 70$ mK.
Detector fabrication done, no physics results yet.

GNO solar neutrino experiment

(Gallium Neutrino Observatory)
Neutrino detection via

$$^{71}Ga + \nu_e \longrightarrow {}^{71}Ge + e^-$$

What is measured is the EC back decay

$$^{71}Ge + e^- \longrightarrow {}^{71}Ga + \nu_e$$

Gas proportional counters:

- detection efficiency only ~ 70%
- major contribution to systematic errors due to escape of Auger electrons and X-rays.

To improve both, LTDs using Ir/Au SPTs are being tested.

4π - geometry to avoid escape of Auger-electrons or X-rays:

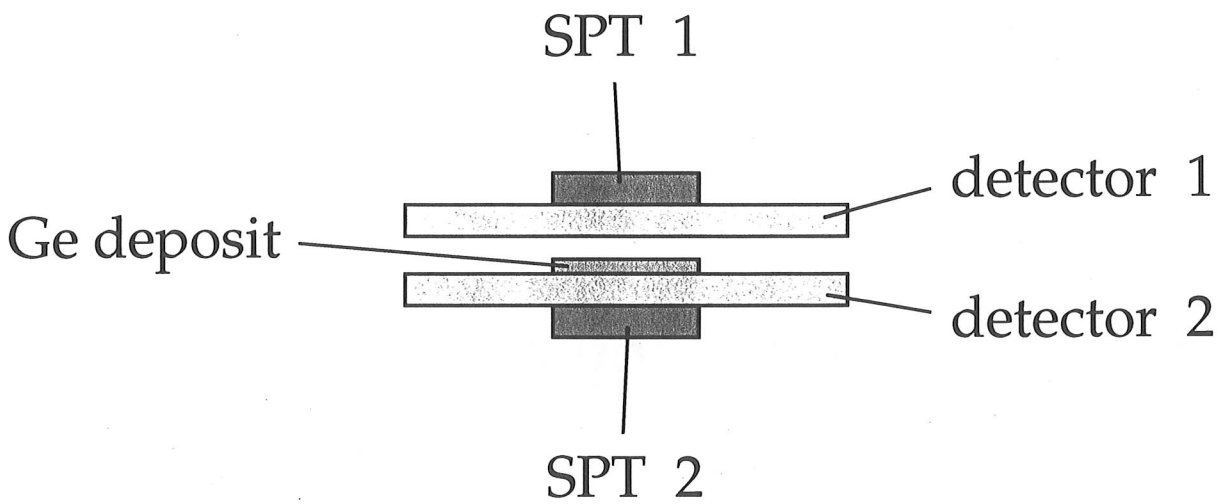

Two sapphire absorbers, 20 x 10 x 0.5 mm^3 each
$\Longrightarrow$ detection efficiency near 100%.

$$\Delta E_{FWHM} \sim 120 \text{ eV} \ @ \ 1.30 \text{ keV} \ \text{(L-capture)}$$
$$\sim 330 \text{ eV} \ @ \ 10.37 \text{ keV} \ \text{(K-capture)}$$

(TU Munich)

IV.5 Dark matter search

Dark matter in form of weakly interacting massive particles (WIMPs):
detection via elastic scattering off nuclei.

- Low energetic recoil nuclei: low ionisation or scintillation efficiency
  $\Longrightarrow$ low temperature calorimeters best choice (detect full deposited energy).
- Expected event rates: ~ 10^{-3} - 1 /kg/keV/day
  $\Longrightarrow$ large detector mass needed.
- Expected energy transfer: few keV
  $\Longrightarrow$ low energy threshold!
- Experiments are background limited
  $\Longrightarrow$ radiopure materials,
  $\Longrightarrow$ high energy resolution to understand the background,
  $\Longrightarrow$ background rejection.

<u>Two DM experiments using SPTs:</u>

CDMS (Cryogenic Dark Matter Search)
CRESST (Cryogenic Rare Event Search using Superconducting Thermometers)

CDMS

100 g Si or 250 g Ge absorbers (76 mm Ø x 10 mm),
W SPTs, $T_C \sim 70$ mK, operated in ETF mode.
Al phonon collectors (however, efficiency only 6%)
«QET» (quasiparticle-trap assisted electro-thermal feedback transition-edge sensors).
Background rejection by simultaneous measurement of ionisation and nonthermal phonons. Ionisation

- low for nuclear recoils (WIMPs, neutrons)
- high for electron recoils (almost all background).

«Dead layer» due to incomplete charge collection
⇒ timing information to reject events near surface.

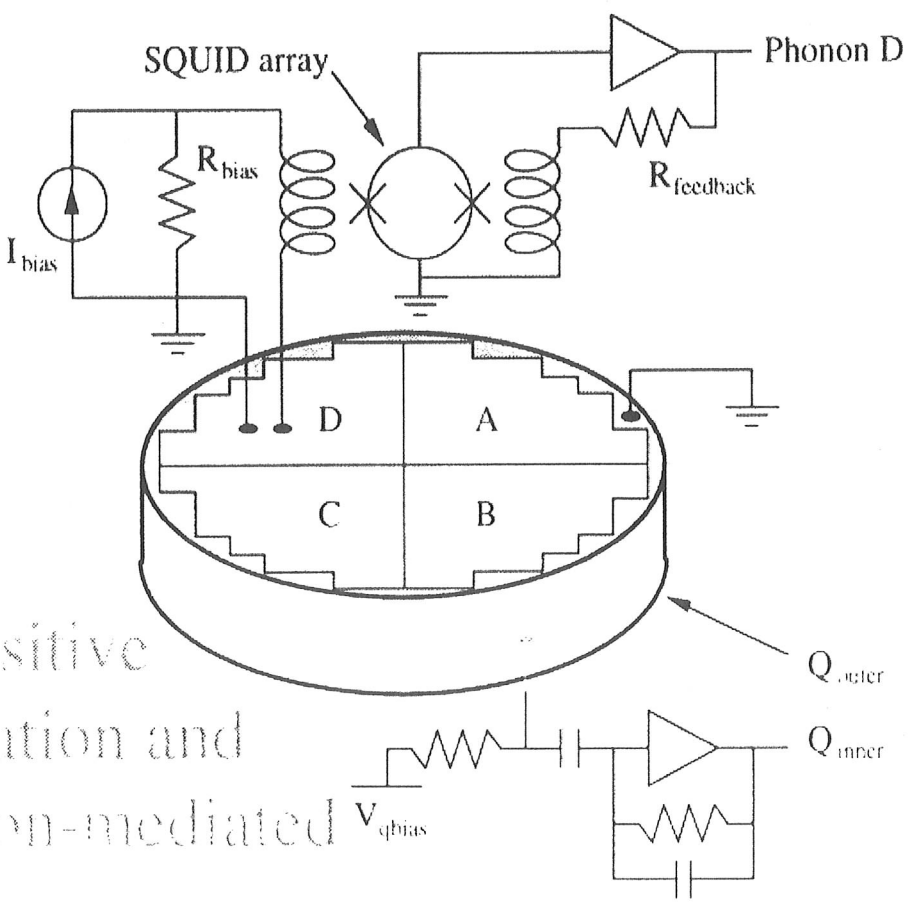

Z-sensitive
*I*onization and
*P*honon-mediated

CDMS detector performance

- Energy resolution - no actual data available
- Baseline noise ~ 500 eV
- Energy threshold ~ 3 keV
- Background rejection restricted below ~ 30 keV due to dead layer.

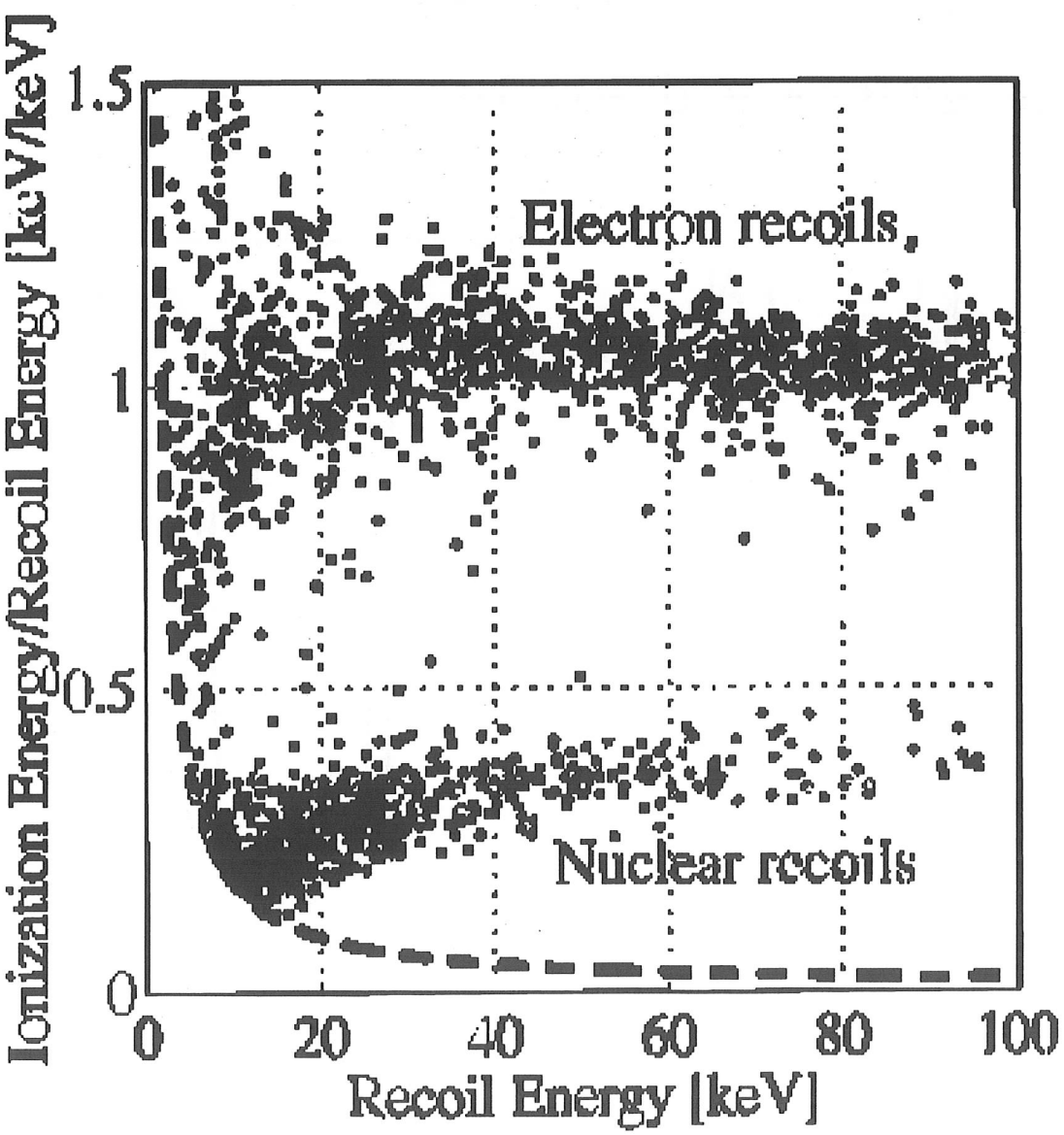

CRESST

- 262 g sapphire absorbers (4 x4 x 4 cm^3)
- W SPTs, T_C ~ 15 mK, operated in conventional or ATF mode.
- No background rejection, high background.

Detector performance

ΔE_{FWHM} = 133 eV @ 1.5 keV

Energy threshold ~ 400 eV

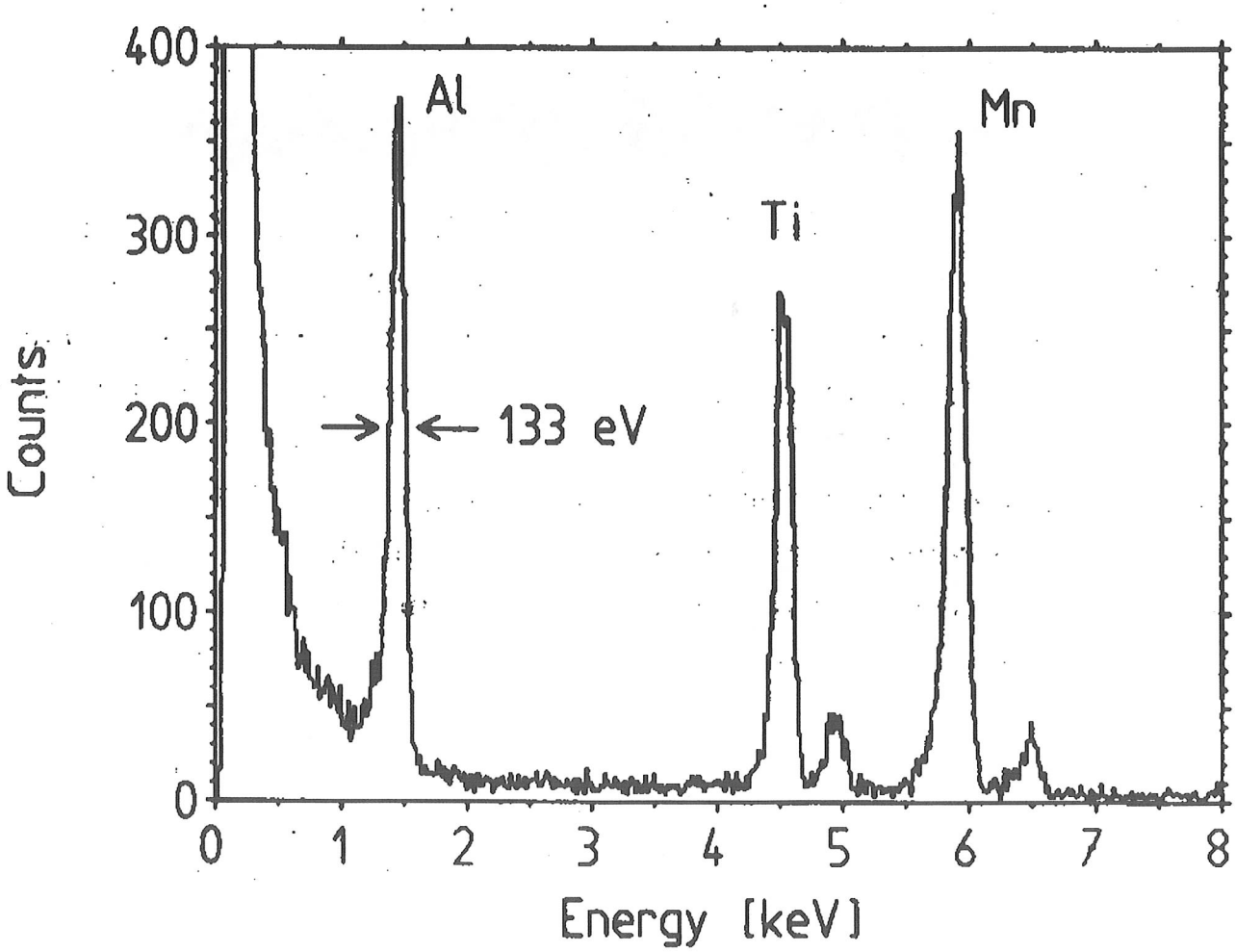

Background rejection planned by simultaneous measurement of nonthermal phonons and scintillation light:

Scintillating absorber crystal with W-SPT
+ additional small calorimeter as light detector, with W-SPT and light absorbing coating.

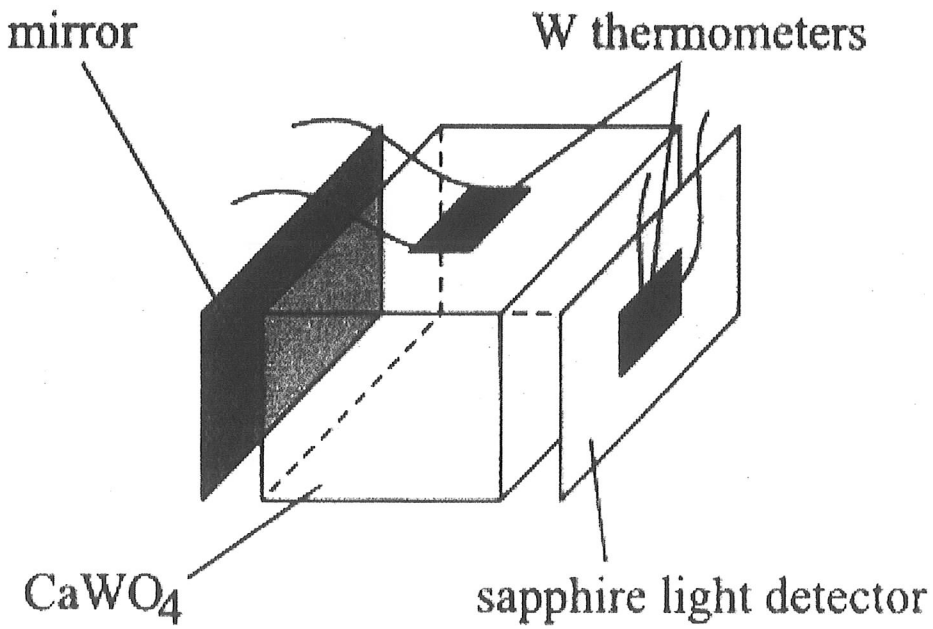

Prototype detector with 6 g $CaWO_4$ absorber
+ sapphire light detector:
rejection efficiency > 99.7% above 15 keV

Detector with 360 g $CaWO_4$ absorber under preparation.

Besides, high efficiency of W/Al bilayers as phonon collectors has been demonstrated.